EBioMedicine 62 (2020) 103134

Contents lists available at ScienceDirect

EBioMedicine

journal homepage: www.elsevier.com/locate/ebiom

Research paper

Targeting metabolic plasticity in glioma stem cells in vitro and in vivo through specific inhibition of c-Src by TAT-Cx43$_{266-283}$

Sara G. Pelaz[a,b,c], Myriam Jaraíz-Rodríguez[a,b,c], Andrea Álvarez-Vázquez[a,b,c], Rocío Talaverón[a,b,c], Laura García-Vicente[a,b,c], Raquel Flores-Hernández[a,b,c], Marta Gómez de Cedrón[d], María Tabernero[d], Ana Ramírez de Molina[d], Concepción Lillo[a,c], José M. Medina[a,b,c], Arantxa Tabernero[a,b,c,*]

[a] Instituto de Neurociencias de Castilla y León (INCYL), Universidad de Salamanca, Calle Pintor Fernando Gallego 1, Salamanca 37007, Spain
[b] Departamento de Bioquímica y Biología Celular, Universidad de Salamanca, Edificio Departamental, Campus Miguel de Unamuno, Salamanca 37007, Spain
[c] Instituto de Investigación Biomédica de Salamanca (IBSAL), Hospital Virgen de la Vega, 10ª planta, Paseo de San Vicente, 58-182, Salamanca 37007, Spain
[d] Precision Nutrition and Cancer Program, Molecular Oncology and Nutritional Genomics of Cancer Group, IMDEA Food Institute, CEI UAM + CSIC, Carretera de Canto Blanco 8 E, Madrid 28049, Spain

ARTICLE INFO

Article History:
Received 5 March 2020
Revised 24 October 2020
Accepted 2 November 2020
Available online xxx

Keywords:
Cancer metabolism
Brain tumour
Connexin
Glioblastoma stem cells
GLUT-3
Hexokinase-2

ABSTRACT

Background: Glioblastoma is the most aggressive primary brain tumour and has a very poor prognosis. Inhibition of c-Src activity in glioblastoma stem cells (GSCs, responsible for glioblastoma lethality) and primary glioblastoma cells by the peptide TAT-Cx43$_{266-283}$ reduces tumorigenicity, and boosts survival in preclinical models. Because c-Src can modulate cell metabolism and several reports revealed poor clinical efficacy of various antitumoral drugs due to metabolic rewiring in cancer cells, here we explored the inhibition of advantageous GSC metabolic plasticity by the c-Src inhibitor TAT-Cx43$_{266-283}$.

Methods: Metabolic impairment induced by the c-Src inhibitor TAT-Cx43$_{266-283}$ in vitro was assessed by fluorometry, western blotting, immunofluorescence, qPCR, enzyme activity assays, electron microscopy, Seahorse analysis, time-lapse imaging, siRNA, and MTT assays. Protein expression in tumours from a xenograft orthotopic glioblastoma mouse model was evaluated by immunofluorescence.

Findings: TAT-Cx43$_{266-283}$ decreased glucose uptake in human GSCs and reduced oxidative phosphorylation without a compensatory increase in glycolysis, with no effect on brain cell metabolism, including rat neurons, human and rat astrocytes, and human neural stem cells. TAT-Cx43$_{266-283}$ impaired metabolic plasticity, reducing GSC growth and survival under different nutrient environments. Finally, GSCs intracranially implanted with TAT-Cx43$_{266-283}$ showed decreased levels of important metabolic targets for cancer therapy, such as hexokinase-2 and GLUT-3.

Interpretation: The reduced ability of TAT-Cx43$_{266-283}$–treated GSCs to survive in metabolically challenging settings, such as those with restricted nutrient availability or the ever-changing in vivo environment, allows us to conclude that the advantageous metabolic plasticity of GSCs can be therapeutically exploited through the specific and cell-selective inhibition of c-Src by TAT-Cx43$_{266-283}$.

Funding: Spanish Ministerio de Economía y Competitividad (FEDER BFU2015-70040-R and FEDER RTI2018-099873-B-I00), Fundación Ramón Areces. Fellowships from the Junta de Castilla y León, European Social Fund, Ministerio de Ciencia and Asociación Española Contra el Cáncer (AECC).

1. Introduction

Glioblastoma (World Health Organization grade IV glioma) is the most common and aggressive primary brain cancer, with a median survival of 16 months [1]. A subset of cells within these tumours, termed glioma or glioblastoma stem cells (GSCs), displays high tumorigenic capacity and resistance to conventional therapies, and is therefore considered responsible for recurrence [2,3]. The GSC phenotype is dynamic and can be acquired by non-GSCs in response to challenging conditions, suggesting that the inherent cancer cell plasticity is a relevant target for treatment [4,5]. These challenging conditions, which include hypoxia, an acidic environment, and metabolic stress, promote the enrichment of the highly tumorigenic GSC population [5-7]. In this regard, an important feature of cancer stem cells, and particularly of GSCs, is their metabolic plasticity, which allows

* Corresponding author.
E-mail address: ataber@usal.es (A. Tabernero).

https://doi.org/10.1016/j.ebiom.2020.103134

Research in context

Evidence before this study

The peptide TAT-Cx43$_{266-283}$ inhibits the oncogenic activity of c-Src specifically in glioblastoma stem cells and decreases their survival, invasion, and tumorigenicity, boosting the survival of preclinical models. Notably, c-Src can regulate glucose and mitochondrial metabolism through several mechanisms. Metabolic plasticity is necessary for glioblastoma establishment and development, and several proteins involved in this plasticity have been identified as potential drug targets. However, these proteins are shared by healthy brain cells, such as neural stem cells, astrocytes and neurons, and specific inhibition of these targets in glioblastoma cells while sparing healthy brain cells remains elusive.

Added value of this study

We found that TAT-Cx43$_{266-283}$ inhibits the metabolic plasticity needed by glioblastoma stem cells, the cells responsible for glioblastoma recurrence and lethality, to exploit the metabolic environment in their favour and thrive in challenging settings. Importantly, glucose metabolism in human and rat healthy brain cells is unaffected by TAT-Cx43$_{266-283}$.

Implications of all the available evidence

Our data support the notion that metabolic plasticity, rather than specific metabolic pathways, constitutes a major targetable vulnerability and confirm the value of TAT-Cx43$_{266-283}$ for glioblastoma therapy alone or in combination with other therapies, including those whose resistance relies on metabolic adaptation.

them to survive nutrient deprivation by conveniently shifting between different metabolic pathways used in energy production and catabolism [8-12]. In particular, glucose metabolism plays a key role in glioblastoma, with glucose restriction promoting GSC enrichment through a two-fold mechanism: direct selection of GSCs, which display the metabolic phenotype required to survive in this environment, and adaptation of some non-GSCs through the acquisition of GSC metabolic features [5]. One of these GSC features is elevated expression of the high-affinity glucose transporter GLUT-3, which is crucial for the tumorigenicity of GSCs and, consequently, for the progression and malignancy of human glioblastomas [5].

Connexin43 (Cx43), the main constituent of gap junctions, has been traditionally considered a tumour suppressor protein because it is downregulated in glioblastoma cells [13,14], including GSCs [15-17]; and because the ectopic expression of Cx43 in glioma cells reduces their rate of proliferation [18] and tumour formation in vivo [19]. However, Cx43 can also play pro-tumorigenic roles in glioma [20]. Indeed, expression of Cx43 in glioma cells can favour glioma invasion [21,22] and drug resistance [23-25], suggesting that very specific tools should be used to selectively mimic the antitumour effects of Cx43. The C-terminal domain of Cx43 interacts with a plethora of molecules and acts as an intracellular signalling hub [26]. This is the case for the proto-oncoprotein c-Src, which is recruited by Cx43 together with its inhibitors CSK and PTEN [27]. This interaction causes the inhibition of c-Src [28] and its downstream oncogenic pathways (for a review see Tabernero et al. [29]). Based on this inhibitory mechanism, we designed a cell-penetrating peptide, TAT-Cx43$_{266-283}$, that recapitulates the inhibition of c-Src by Cx43 [17]. Malignant gliomas have high oncogenic c-Src activity [30]; moreover, cancer stem cells, including GSCs, rely on the activity of this oncoprotein for survival, stemness, and invasion [17,31-36]. Importantly, TAT-Cx43$_{266-283}$ specifically inhibits c-Src activity and consequently exerts potent antitumour effects in primary human glioblastoma cells [35] and in the reversion of the GSC phenotype [17] in vitro and in vivo without affecting healthy brain cells [36]. These studies suggest that the mechanism of the antitumour action of TAT-Cx43$_{266-283}$ involves inhibition of the oncogenic activity of c-Src and not blockade of endogenous Cx43 function. Indeed, the level of Cx43 expression is very low and the activity of c-Src is high in TAT-Cx43$_{266-283}$ target cells, such as GSCs, whereas no effect of TAT-Cx43$_{266-283}$ on cell viability is found in cells with high expression of Cx43 and low activity of c-Src, such as astrocytes [36]. GSCs display a high invasive capacity, which strongly contributes to glioblastoma recurrence [35]. Significantly, by inhibiting c-Src, TAT-Cx43$_{266-283}$ reduces migration, invasion, and survival in human primary GSCs, including freshly removed surgical specimens studied as undissociated glioblastoma blocks [35]. Moreover, TAT-Cx43$_{266-283}$ inhibits c-Src, impairs malignant growth, and enhances survival in mouse models in vivo [36], supporting the translational potential of this peptide for the treatment of glioblastoma.

The relationship between the oncogenic activity of c-Src and glucose metabolism has been known for more than 30 years[37], and during this time numerous studies have delved into the underlying mechanisms. For instance, c-Src can modulate glucose metabolism, either indirectly through master transcription factors, such as c-myc [38] or hypoxia inducible factor 1α (HIF-1α) [39,40], or directly through regulation of the activity of key glucose metabolism proteins, such as hexokinase-2 (HK-2) [41], which traps glucose intracellularly for further metabolism, or glucose-6-phosphate-dehydrogenase (G6PD) [42], the key and rate-limiting enzyme in the pentose phosphate pathway. Moreover, c-Src activity can regulate oxidative phosphorylation of substrates in the mitochondria via phosphorylation of respiration or mitochondrial translation proteins, amongst other mechanisms [43-45].

In addition to a conferred advantage to survive in nutrient-deprived conditions, metabolic plasticity is responsible for resistance to certain cancer treatments, one of the most relevant hallmarks of GSCs [2,3]. For instance, glioblastoma cells adapt to bevacizumab treatment—a common antiangiogenic therapy—by increasing glycolysis [46,47]. Similarly, tumour cells can rewire their metabolism to suit their needs under different environmental conditions, which can negatively affect their response to common antitumoral drugs, such as mTOR [48] and glutaminase inhibitors [49], 5-fluorouracil and metformin, and even to immunotherapy [50]. Consequently, inhibition of this metabolic plasticity is becoming a promising therapeutic target, and cell selectivity is undoubtedly hugely important in the context of brain tumours. Therefore, here we investigated the effect of TAT-Cx43$_{266-283}$, a promising therapeutic peptide against glioblastoma, on GSC metabolism and metabolic plasticity as a meaningful predictor of the success of a future clinical application.

2. Materials and methods

2.1. Animals

Albino Wistar rats and NOD/SCID mice were obtained from the animal facility of the University of Salamanca. All animal procedures were approved by the ethics committee of the University of Salamanca and the *Junta de Castilla y León* and were carried out in accordance with European Community Council Directives (2010/63/UE) and Spanish law (R.D. 53/2013 BOE 34/11,370−420, 2013) for the care and use of laboratory animals.

Mice were maintained singly from the start of the experiments under 12-h light/dark cycles, had free access to food and water at all times, and were monitored for signs of humane endpoints daily,

including changes in behaviour and weight. A total of nine male and female adult mice were used for the in vivo experiments.

2.2. Cells

G166 human GSCs (RRID:CVCL_DG66) and G179 human GSCs (RRID:CVCL_DG69) (both IDH-wt) [51] were obtained from BioRep [17]. Primary G9 human GSCs were obtained from human surgical specimens of glioblastoma patients, as previously described [35]. Unless otherwise stated, the GSCs used in the experiments were G166 GSCs. GSCs were cultured in RHB-A medium (Takara Bio Inc.) supplemented with 2% B27 (Life Technologies), 1% N2 (Life Technologies), 20 ng ml^{-1} EGF, and 20 ng ml^{-1} b-FGF (PeproTech) (complete medium) under adherent conditions, as described by Pollard et al. [52]. Human neural stem cells (NSCs) were obtained from Takara Bio Inc. (ref.: Y40050) [53]. NSCs were cultured in RHB-A medium (Takara Bio Inc.) supplemented with 20 ng ml^{-1} EGF, and 20 ng ml^{-1} b-FGF (PeproTech) (complete medium) under adherent conditions, as described by Hook et al. [53] Culture plates were coated with 10 μg ml^{-1} laminin (Invitrogen, 23,017−015) for 2 h before use. Cells were grown to confluence, dissociated using Accutase (Thermo Fisher), and then split to convenience. We routinely used cultures expanded for no more than 15 passages. For differentiation, G166 GSCs were cultured in RHB-A medium supplemented with 5% FCS, as indicated [52]. Human astrocytes were obtained from NSCs cultured in RHB-A medium supplemented with 1% FCS, as indicated [53].

Primary rat neuron and astrocyte cultures were performed as previously described [54]. Neurons in primary culture were prepared from the forebrains of foetuses at 17.5 days of gestation and cultured in Dulbecco's modified Eagle's medium (DMEM; Sigma-Aldrich, D5523) supplemented with 10% foetal calf serum (FCS; Gibco). One day after plating, cytosine arabinoside was added to avoid glial cell proliferation. Astrocytes in primary culture were prepared from the forebrains of 1- to 2-day-old Wistar rats and cultured in DMEM supplemented with 10% FCS. The cells were maintained at 37 °C in an atmosphere of 95% air/5% CO_2 and with 90−95% humidity.

2.3. Cell treatments

Synthetic peptides (> 85% pure) were obtained from GenScript (Piscataway, NJ, USA). YGRKKRRQRRR was used as the TAT sequence, which enables the cell penetration of peptides [55]. The TAT-$Cx43_{266-283}$ sequence was TAT-AYFNGCSSPTAPLSPMSP (patent ID: WO2014191608A1).

For in vitro and ex vivo studies, the peptides (TAT, as a negative control, and TAT-$Cx43_{266-283}$) were used at 50 μM in culture medium at 37 °C for 24 or 48 h, as indicated. Dasatinib (1 μM) or 0.1% (v/v) DMSO was added to the culture medium at 37 °C for 24 h. To analyse TAT-$Cx43_{266-283}$ internalisation, 50 μM TAT-$Cx43_{266-283}$ fused to biotin at the C terminus (TAT-$Cx43_{266-283}$-B) was added to the culture medium at 37 °C for 30 min and visualised with streptavidin, as previously reported [36]. For in vivo studies in NOD/SCID mice, a single intracranial injection of 1 μl of saline containing 100 μM TAT or 100 μM TAT-$Cx43_{266-283}$ and 5000 GSCs was performed as previously described [36].

In addition to either 50 μM TAT or TAT-$Cx43_{266-283}$ (where indicated), the cell media (pH 7.3) used in the metabolic plasticity study had the following compositions; in the 4-day long experiments: Earl's Balanced Salt Solution (EBSS) containing 5.6 mM glucose (Video 1); EBSS containing 0.4 mM glycine, 4 mM glutamine, 4 mM serine, and essential amino acids (MEM Amino Acids Solution; Gibco, 11,130,036; Video 2); for all other experiments: EBSS containing 14 mM glucose (glucose-only medium); EBSS containing 4 mM glutamine, essential amino acids, and non-essential amino acids (MEM Non-Essential Amino Acids Solution; Gibco, 11,140,050) (amino acid-only medium); and EBSS containing 14 mM glucose, 4 mM glutamine, essential amino acids, and non-essential amino acids (glucose and amino acid medium).

2.4. Ex vivo 2-NBDG uptake assay

GSC−organotypic brain slice co-cultures were incubated overnight to ensure GSC engraftment into the brain slices. The co-culture brain slices were then incubated with 50 μM TAT or TAT-$CX43_{266-283}$ for 48 h. On the day of the assay, the brain slices were incubated for 30 min in glucose-free medium (RPMI; Sigma-Aldrich) and subsequently for 1 h in glucose-free medium supplemented with 146 μM 2-NBDG (2-[N-(7-*nitrobenz*-2-*oxa*-1,3-*diazol*-4-*yl*) *amino*]−2-deoxy-D-glucose). The brain slices were then washed with ice-cold phosphate-buffered saline (PBS) and mounted for confocal microscopy with SlowFade Gold Antifade reagent (Life Technologies). Images were taken on a Leica DM-IRE2 confocal microscope. For 2-NBDG uptake analysis, regions of interest (ROIs) were generated with the 'Wand' tool (ImageJ) in the GSC images and the mean grey values of the ROIs were measured in the corresponding 2-NBDG images.

2.5. Extracellular lactate

Extracellular lactate was determined using a commercial kit (Sigma-Aldrich, mak064) and the cell medium was filtered through 10,000 Nominal Molecular Weight Limit (NMWL) filters to eliminate possible extracellular lactate dehydrogenase that would degrade lactate, following the manufacturer's instructions. Results were normalised to the protein content of the samples.

2.6. GSC−organotypic brain slice co-cultures

Organotypic brain slice cultures were prepared as previously described [56]. Briefly, 350-μm-thick brain slices were obtained from neonatal Wistar rats and cultured onto cell culture inserts in DMEM supplemented with 10% horse serum and glucose (final concentration: 33 mM). The medium was replaced three times a week and slices were maintained in culture for 19−20 DIV. Then, 2500 G166 GSCs fluorescently labelled with CellTracker Red CMPTX (Life Technologies) were placed onto each brain slice and maintained in culture for the indicated time.

2.7. Hexokinase activity assay

The hexokinase (HK) activity of cells was determined using a commercial kit (Abcam, ab136957) following the manufacturer's instructions. Cells were incubated for 30 min in glucose-free medium (RPMI, Sigma-Aldrich) prior to the assay. The absorbence of the cell lysates was measured in a microplate fluorometer at two time points within the linear range of the reaction and normalised to the protein content of the samples.

2.8. In vitro 2-NBDG and 6-NBDG uptake assay

The cells were incubated with the peptides when confluence was reached for the indicated time. Then, they were incubated for 30 min in glucose-free medium (RPMI, Sigma-Aldrich) and subsequently for 1 h in glucose-free medium supplemented with 146 μM of the fluorescent glucose analogue 2-NBDG (2-[N-(7-*nitrobenz*-2-*oxa*-1,3-*diazol*-4-*yl*) *amino*]−2-deoxy-D-glucose), which comprises a glucose moiety with an N-nitrobenzoxadiazole (NBD)-amino group (fluorophore) at carbon 2 replacing the hydroxyl group, or 6-NBDG (6-[N-(7-*nitrobenz*-2-*oxa*-1,3-*diazol*-4-*yl*) *amino*]−6-deoxy-D-glucose), whose NBD-amino group is placed at carbon 6 and can therefore not be phosphorylated by HKs [57] (Thermo Fisher). The cells were then washed with ice-cold PBS and lysed, scraped, and homogenised by 10 passages through a 25-gauge needle. Homogenates were centrifuged and

the fluorescence of supernatants was measured in a microplate reader (Appliskan; Thermo Electron Corporation, Thermo Scientific). For 2-NBDG uptake, a standard curve was generated by measuring the fluorescence of a range of 2-NBDG concentrations in lysis buffer (1% Nonidet P-40, 1% sodium deoxycholate, 40 mM KCl, and 20 mM Trizma Base [Sigma-Aldrich], pH 7.4). 2-NBDG and 6-NBDG uptake was normalised to protein content of the samples.

2.9. Image analysis

Images were analysed using Fiji Software [58], available at http://rsbweb.nih.gov/ij/. For in vitro and ex vivo experiments, details of the image analysis are specified in the corresponding figure legend. In the in vivo study, maximum z projections were obtained from confocal stack images. Projections were subjected to background subtraction and the mean grey value of the image was obtained. Non-specific staining was measured in three identically sized regions from each image and subtracted from the corresponding mean grey value.

2.10. Immunofluorescence

For in vitro studies, immunofluorescence was performed as previously described [17]. Briefly, cells were incubated with MitoTracker Red CMXRos (final concentration: 100 nM in culture medium; Invitrogen, M7512) for 1 h at 37 °C where indicated and then fixed in methanol for 10 min at −20 °C. The cells were then rinsed in PBS and incubated for 1 h in blocking solution (PBS containing 10% FCS, 0.1 M lysine, and 0.02% azide). The samples were incubated overnight at 4 °C with the indicated primary antibody prepared in blocking/permeabilisation solution (with 0.1% Triton X-100): rabbit polyclonal antibody against GLUT-1 (1:250; Millipore 07−1401 or Abcam ab652; RRID:AB_1587074 and RRID:AB_305540, respectively), rabbit monoclonal antibody against HK-1 (1:200; Cell signalling Technology 2024, RRID:AB_2116996), or mouse monoclonal antibody against HK-2 (1:100; Thermo Fisher MA5−15679, RRID:AB_10986812). After repeated washes, they were incubated for 75 min with the corresponding secondary antibody prepared in blocking/permeabilisation solution: anti-rabbit IgG or anti-mouse IgG Alexa Fluor 488-, Alexa Fluor 594-, or Alexa Fluor 647-conjugated antibodies (1:1000; Life Technologies). Finally, nuclear DNA was stained with 1 μg ml^{-1} 4′,6-diamidino-2-phenylindole (DAPI) for 1 min. Cells were mounted using SlowFade Light antifade (Life Technologies) and imaged on an inverted Zeiss Axio Observer Z1 microscope for Live-Cell Imaging (Carl Zeiss Microscopy) coupled to an AxioCam MRm camera and Zeiss Apotome (optical sectioning structured illumination microscopy; https://www.zeiss.com/microscopy/int/solutions/reference/all-tutorials/optical-sectioning/apotome-operation.html).

For in vivo studies, sections were washed in PBS and incubated for 1 h in blocking/permeabilisation solution. Then, the sections were incubated overnight at room temperature with the indicated primary antibody prepared in blocking/permeabilisation solution: mouse monoclonal antibody against HK-2 (1:100; Thermo Fisher MA5−15,679, RRID:AB_10986812) or mouse monoclonal antibody against GLUT-3 (1:100; Santa Cruz Biotechnology sc-74497, RRID: AB_1124974). After repeated washes, the sections were incubated for 2 h with the corresponding secondary antibody prepared in blocking/permeabilisation solution: anti-rabbit IgG or anti-mouse IgG Alexa Fluor 488- or Alexa Fluor 647-conjugated antibodies (1:500; Life Technologies). Finally, nuclear DNA was stained with DAPI for 4 min and samples were imaged by confocal microscopy on a Leica TCS SP2 microscope. Briefly, 8-bit images from consecutive focal planes (1 μm along the z axis) were scanned with a pinhole aperture of 1 Airy Unit.

2.11. Xenograft orthotopic glioblastoma mouse model

Human G166 GSCs stably transfected with pcDNA3.1-mCherry plasmid [59] (cytomegalovirus promoter for constitutive expression of mCherry; Addgene plasmid #128744;) or human G166 GSCs labelled with a Red Fluorescent Cell kit PKH26 (Sigma-Aldrich) were intracranially implanted into the brains of NOD/SCID mice as previously described [36]. Briefly, mice were anaesthetised by isoflurane inhalation, placed in a stereotaxic frame, and window-trephined in the parietal bone. A unilateral intracerebral injection to the right cortex was performed with a Hamilton microsyringe. Cellular suspensions were kept on ice while the surgery was being performed. Then, 1 μl of physiological saline containing 5000 cells was injected into the cortex of adult mice placed in a stereotaxic frame at the following coordinates: 5 mm caudal to bregma, 4 mm lateral, and 2 mm deep. The needle was held in place for 1 min after cell injection.

After 7 days, the animals were transcardially perfused under deep anaesthesia (pentobarbital 120 mg kg^{-1}, 0.2 ml) with 15 ml of physiological saline followed by 25 ml of 4% paraformaldehyde in 0.1 M phosphate buffer (pH 7.4). Brainstems were removed and cryoprotected by immersion in a solution of 30% sucrose in PBS until they sank. Then, 20−40-μm-thick coronal sections were obtained with a cryostat to be processed for immunostaining.

2.12. MTT assay

Cells were incubated in the dark for 75 min with culture medium containing 0.5 mg ml^{-1} MTT (Sigma-Aldrich). The cells were then carefully washed with PBS once and incubated for 10 min in the dark in DMSO with mild shaking. Absorbance was measured at a wavelength of 570 nm using a microplate reader.

2.13. Oxygen consumption rate and extracellular acidification rate

The oxygen consumption rate (OCR) and extracellular acidification rate (ECAR) were monitored as indicators of mitochondrial respiration and glycolytic function, respectively, with an XF96 Extracellular Flux analyser using an XF Cell Mito Stress Test kit and XF Glycolysis Stress Test kit according to the manufacturer's instructions (Seahorse Biosciences). For the Mito Stress Test and Glyco Stress Test kits, seeding numbers were optimised to 1.6×10^4 cells/well and 8×10^3 cells/well for GSCs, to 6.36×10^4 and 3.18×10^4 cells/well for neurons, and to 2.65×10^4 and 9.93×10^3 cells/well for astrocytes, respectively.

For the mitochondrial stress test, cells were plated in XF96 plates and treated with TAT or TAT-Cx43$_{266-283}$ as indicated. Prior to the assay, the regular culture media was replaced with Base medium (Seahorse Bioscience) supplemented with 1 mM pyruvate, 2 mM glutamine, and 10 mM glucose and the cells were incubated without CO_2 for 1 h. Basal rate measurements were taken and then mitochondrial respiratory chain drugs were added according to Mito Stress Test kit specifications. Next, 1.5 μM oligomycin was used to block ATP-linked oxygen consumption, 0.4 μM carbonyl cyanide-*P*-trifluoromethoxyphenylhydrazone (FCCP; an uncoupling agent) was used to obtain maximal respiration, and 0.5 μM rotenone/antimycin A was used to inhibit complexes I and III to stop all mitochondrial respiration.

For glycolysis analysis, Base medium supplemented with 0.5 mM pyruvate and 2 mM glutamine was used and cells were incubated without CO_2 for 1 h. In accordance with Glycolysis Stress Test kit specifications, 10 mM glucose was injected to stimulate glycolysis, 1.5 μM oligomycin was then injected to obtain the maximal glycolytic capacity upon oxygen consumption inhibition, and 50 mM 2-deoxy-D-glucose (2-DG) was finally used to shut down all glycolysis.

OCR and ECAR were measured three times after the injection of each drug. At least six replicates per condition were performed in

each experiment. Parameter calculations were performed using the Seahorse XF Cell Test Report Generator provided by Seahorse Biosciences. Non-mitochondrial respiration is the minimum rate measurement after Rot/AA injection; basal respiration is the oxygen consumption used to meet cellular ATP demand, calculated by subtracting non-mitochondrial OCR from the measurement prior to oligomycin addition; proton leak is calculated by subtracting the non-mitochondrial OCR from the minimum rate measurement after oligomycin injection; ATP-linked respiration is calculated by subtracting the minimum rate measurement after oligomycin injection from the last rate measurement before oligomycin injection; maximal respiration capacity is calculated by subtracting non-mitochondrial respiration from the maximum rate measurement after FCCP injection; and spare respiratory capacity, the ability to respond to an energetic demand, is calculated as the difference between maximal and basal respirations. Non-glycolytic acidification is the last rate measurement prior to glucose injection, glycolysis is calculated as the maximum rate measurement before oligomycin injection minus the last rate measurement before glucose injection, glycolytic capacity is calculated as the maximum rate measurement after oligomycin injection minus the last rate measurement before glucose injection, and glycolytic reserve is calculated as glycolytic capacity minus glycolysis.

2.14. Real-time quantitative polymerase chain reaction

DNA from GSCs was extracted with a QIAamp DNA Mini kit (Qiagen) following the manufacturer's instructions. DNA concentration and quality were analysed in a NanoDrop 2000 spectrophotometer.

Real-time quantitative polymerase chain reaction (PCR) reactions were performed in triplicate in 96-well plates in a QuantStudio 7 Flex Real-Time PCR System (Thermo Fisher). Equal initial amounts of total DNA were amplified in all conditions. A PCR master mix was prepared for each sample containing 1 μL DNA, 1 μM of forward and reverse primers, and 12.5 μL of SYBR® Green Master Mix (Life Technologies) in a 25-μL reaction mix.

The primers used for amplification were: *mt-ND1* (mitochondrial DNA gene) forward 5′-CCC TAA AAC CCG CCA CAT CT-3′ and reverse 5′-GAG CGA TGG TGA GAG CTA AGG T-3′; and *β−2-μglobulin* [60] (nuclear DNA gene) forward 5′-TGC TGT CTC CAT GTT TGA TGT ATC T-3′ and reverse 5′-TCT CTG CTC CCC ACC TCT AAG T-3′. Negative control reactions for each set of primers were performed in the absence of cDNA template. Reaction products were run on a 2% agarose gel containing Syber Safe DNA gel stain (Invitrogen) to ascertain correct primer amplification (Supplementary Fig. 2). Real-time PCR results were analysed as described by Pfaffl et al. [61]

2.15. siRNA transfection

Cells were transfected with a validated non-targeting siRNA or with an siRNA specific for HK-1 (5′-CAC GAT GTA GTC ACC TTA CTA-3′) together with an siRNA specific for HK-2 (5′-CTG GCT AAC TTC ATG GAT A-3′) [41]. Transfections were performed with Lipofectamine 2000 reagent according to the manufacturer's instructions.

The reduction in protein expression was assessed by western blot analysis 48 and 72 h after transfection (Supplementary Fig. 1f). Cell treatments were performed 48 h after transfection, and glucose uptake analyses 72 h after transfection.

2.16. Time-lapse microscopy

GSCs were plated at 5×10^4 cells/well in 12-well plates. Once the cells had attached, TAT or TAT-Cx43$_{266-283}$ was added at 50 μM for 24 h. Then, the cell culture media was changed to the indicated media including 50 μM TAT or TAT-Cx43$_{266-283}$ and the cells were allowed to equilibrate for 1 h in the microscope incubator before imaging. The cells were recorded by time-lapse live-cell imaging for 24 h. Every 10 min, phase-contrast microphotographs of each experimental condition were taken for live-cell imaging with an inverted Zeiss Axio Observer Z1 microscope coupled to an AxioCam MRm camera. The system included an automated XY stage controller and a humidified incubator set at 37 °C and 5% CO_2.

2.17. Transmission electron microscopy

Cell culture preparations were fixed in 2% formaldehyde and 2% glutaraldehyde in phosphate buffer for 30 min at 4 °C. Samples were then post-fixed with 1% osmium tetroxide in water, dehydrated through a graded ethanol series, and embedded in Epoxy EMbed-812 resin (Electron Microscopy Sciences). Ultrathin sections were obtained with a Leica EM UC7 ultramicrotome, contrasted with uranyl acetate and lead citrate, and analysed using a Tecnai Spirit Twin 120 kV electron microscope with a CCD Gatan Orius SC200D camera with DigitalMicrograph™ software. Procedures were performed at the Electron Microscopy Facilities-NUCLEUS of the University of Salamanca.

2.18. Western blotting

Western blotting was performed as described previously [35]. Briefly, equal amounts of proteins across conditions were separated on NuPAGE Novex Bis-Tris 4−12% Midi gels (Life Technologies) at room temperature and constant voltage. Proteins were transferred to a nitrocellulose membrane (iBlot Gel Transfer Stacks Nitrocellulose) using an iBlot dry blotting system (Life Technologies). After blocking, the membranes were incubated overnight at 4 °C with primary antibodies: mouse monoclonal antibody against α-actinin (1:1000; Millipore MAB1682, RRID:AB_94325), mouse monoclonal antibody against G6PD (1:250; Santa Cruz Biotechnology sc-373886, RRID:AB_10918100), mouse monoclonal antibody against glyceraldehyde phosphate dehydrogenase (GAPDH; 1:5000; Thermo Fisher Scientific AM4300, RRID:AB_437392), rabbit polyclonal antibody against GLUT-1 (1:500−1:1000; Millipore 07−1401, RRID:AB1587074), mouse monoclonal antibody against GLUT-3 (1:100; Santa Cruz Biotechnology sc-74497, RRID:AB_1124974), rabbit polyclonal antibody against HIF-1α (1:200; Novus Biologicals NB100−479, RRID:AB_10000633), rabbit monoclonal antibody against HK-1 (1:250; Cell signalling Technology 2024, RRID:AB_2116996), mouse monoclonal antibody against HK-2 (1:500; Thermo Fisher MA5-15679, RRID:AB_10986812), mouse monoclonal antibody against RPL-19 (1:200; Santa Cruz Biotechnology sc-100830, RRID:AB_2181588), rabbit polyclonal antibody against Sox-2 (1:500; Abcam ab97959, RRID:AB_2341193), Total OXPHOS Rodent WB Antibody Cocktail against NDUFB8 (complex I), SDHB (complex II), UQCRC2 (complex III), MTCO1 (complex IV), and ATP5A (complex V) (1:250; Abcam ab110413, RRID:AB_2629281), and mouse monoclonal antibody against α-tubulin (1:1000; Sigma-Aldrich T9026, RRID:AB_477593). After extensive washing, the membranes were incubated with peroxidase-conjugated anti-rabbit IgG or anti-mouse IgG antibodies (1:5000; Jackson ImmunoResearch) and developed with a chemiluminescent substrate (Western Blotting Luminol Reagent; Santa Cruz Biotechnology) in a MicroChemi imaging system (Bioimaging Systems). Original and replicate blots are shown in the Supplementary Figures. α-actinin, GAPDH, RPL-19 and α-tubulin were used as loading controls.

2.19. Statistical analysis

Results are expressed as the means ± *s*.e.m. The number of technical replicates and independent experiments is indicated for each experiment in its corresponding figure and figure legend, and was determined according to the previous experience of the research group. For comparison between two groups, data were analysed by

two-tailed Student's *t*-test. When more than two groups were compared, data were analysed by one-way ANOVA, and confidence intervals (95%) and significance were corrected for multiple comparisons with the Tukey test. In all cases, values were considered significant when $P < 0.05$. Exact *P* values can be found in Supplementary Table 1.

2.20. Role of the funding sources

The funding sources had no involvement in study design, in the collection, analysis, and interpretation of data, in the writing of the report, or in the decision to submit the paper for publication.

3. Results

3.1. TAT-Cx43$_{266-283}$ decreases glucose uptake selectively in GSCs

Because the highly efficient glucose uptake in GSCs confers these cells with a competitive advantage within the brain environment [5], we first analysed the effect of TAT-Cx43$_{266-283}$ on glucose transport and uptake. Glucose transport was evaluated in GSCs using the non-metabolisable fluorescent glucose analogue 6-NBDG, whose uptake reflects gradient-driven influx through glucose transporters [57]. We found no differences in 6-NBDG transport (146 μM for 1 h) between controls (untreated condition [Control] and negative control [TAT]) and TAT-Cx43$_{266-283}$–treated GSCs (50 μM, 24 h), suggesting that TAT-Cx43$_{266-283}$ does not modify glucose transport under these experimental conditions (Fig. 1a).

To confirm this result, we analysed GLUT-1, the main glucose transporter. GLUT-1 levels in GSCs were not affected by TAT-Cx43$_{266-283}$ treatment (Fig. 1b, Supplementary Fig. 1a and b). The levels of GLUT-3, another glucose transporter frequently co-opted by cancer cells [5,62], were also not affected by TAT-Cx43$_{266-283}$ under these experimental conditions (Fig. 1b).

Next, we measured glucose uptake with the non-metabolisable fluorescent glucose analogue 2-NBDG, which is phosphorylated by HK and trapped intracellularly. The results showed that TAT-Cx43$_{266-283}$ decreased glucose uptake in G166 GSCs by ~30% (Fig. 1c and d). Similar results were obtained in G179 GSCs and in primary human G9 GSCs, whereas uptake was unchanged in differentiated G166 glioblastoma cells, human NSCs, human astrocytes, rat astrocytes, and rat neurons (Fig. 1c and d, and Supplementary Fig. 1c). TAT-Cx43$_{266-283}$-B is internalised by G166 GSCs and, to a lesser extent, by rat astrocytes, but not significantly so by neurons [36]. In the present study, we confirmed that TAT-Cx43$_{266-283}$-B is internalised by human G179 GSCs and, to a lesser extent, by human astrocytes (Supplementary Fig. 1d). Interestingly, the internalisation was decreased in differentiated glioblastoma cells and NSCs as compared to GSCs (Supplementary Fig. 1d). These results add to the evidence from our previous reports that TAT-Cx43$_{266-283}$ specifically targets GSCs [36], including G9 and other primary GSCs [35]. Moreover, TAT-Cx43$_{266-283}$ reduced HK activity (Fig. 1e) without altering the levels of HK-1 and HK-2 in GSCs (Fig. 1b). Immunofluorescence assays confirmed similar levels of HK-1 and HK-2 (Fig. 1f and the quantification in Supplementary Fig. 1e) and showed that both HKs localised more compactly around the nuclei of GSCs treated with TAT-Cx43$_{266-283}$ (Fig. 1f). Because HK-1 and HK-2 activities are enhanced by c-Src phosphorylation [41], the TAT-Cx43$_{266-283}$–induced inhibition of c-Src [17,35] might hinder HK activity. Indeed, inhibition of c-Src activity by dasatinib, a commonly used c-Src inhibitor, reduced glucose uptake in G166 and G179 GSCs without altering glucose uptake in differentiated glioblastoma cells, human NSCs, or human astrocytes (Fig. 1g).

To further confirm the involvement of HK in the effect of TAT-Cx43$_{266-283}$, HK-1 and HK-2 expression was knocked down by siRNA (Supplementary Fig. 1f). The results showed that the effect of TAT-Cx43$_{266-283}$ on glucose uptake in GSCs is reduced when the expression of HK-1 and HK-2 is silenced (Fig. 1h). Taken together, these data indicate that 24-h treatment with TAT-Cx43$_{266-283}$, via inhibition of c-Src activity, reduces glucose uptake selectively in GSCs through decreased HK activity, without affecting glucose transport or the protein levels of GLUT-1, GLUT-3, HK-1, or HK-2.

3.2. TAT-Cx43$_{266-283}$ reduces mitochondrial metabolism without increasing glycolysis in GSCs

Because we found that TAT-Cx43$_{266-283}$ altered the localisation of HKs (Fig. 1f), which are frequently associated with mitochondria [41,63], we used a mitochondrial dye to track the cellular distribution of these organelles. Importantly, these images revealed that TAT-Cx43$_{266-283}$ treatment (50 μM, 24 h) modified the localisation of mitochondria in GSCs (Fig. 2a, and Supplementary Fig. 2a). Indeed, the distance from the furthest mitochondria to the nucleus was reduced in GSCs after TAT-Cx43$_{266-283}$ treatment (Fig. 2b), suggesting altered mitochondrial trafficking. Similar results were obtained in G179 GSCs (Fig. 2b). However, no changes in mitochondrial localisation were found in differentiated G166 glioblastoma cells, human NSCs and human and rat astrocytes (Fig. 2b and c, and Supplementary Fig. 2a). The changes in mitochondrial localisation found in TAT-Cx43$_{266-283}$-treated GSCs might arise from the inhibition of c-Src activity, as similar results were obtained with dasatinib (Supplementary Fig. 2b).

In addition, the area occupied by mitochondria per cell was reduced in TAT-Cx43$_{266-283}$–treated GSCs (Supplementary Fig. 2c). To establish if this result was due to the spatial rearrangement of mitochondria or to a decrease in cell size or in mitochondrial mass, we analysed the cell area, perimeter and circularity of GSCs and we performed western blotting against subunit proteins from each of the five complexes of the electron transport chain (ETC) involved in oxidative phosphorylation (OXPHOS). Treatment with TAT-Cx43$_{266-283}$ did not affect the cell area, perimeter and circularity of the cells (Supplementary Fig. 2d), or the relative abundance of ETC complexes in GSCs (Fig. 2d and Supplementary Fig. 2e). Similarly, quantification of mitochondrial DNA relative to nuclear DNA by real-time quantitative PCR did not reveal any changes (Fig. 2e and Supplementary Fig. 2f), confirming that 24-h TAT-Cx43$_{266-283}$ treatment induced a spatial rearrangement in the mitochondrial network of GSCs without changes in total mitochondrial mass. To further characterise the effect of TAT-Cx43$_{266-283}$ on GSC mitochondria, we performed transmission electron microscopy. The images revealed that, in mitochondria from TAT-Cx43$_{266-283}$–treated GSCs, the matrix was more electron-dense and the outer membrane and cristae less defined, indicative of structural changes associated with the previous observations (Fig. 2f; the blue arrowheads indicate the outer membrane, the cristae are coloured).

To determine if the distinct cellular localisation and ultrastructure observed in mitochondria from GSCs treated with TAT-Cx43$_{266-283}$ affected mitochondrial function, we measured the GSC oxygen consumption rate (OCR) as an indicator of mitochondrial respiration in a Seahorse XF analyser [64]. As shown in Fig. 2g, GSCs treated with TAT-Cx43$_{266-283}$ had a lower basal OCR (minutes 0–18), as well as a lower response to mitochondrial stimulation with FCCP (minutes 42–55). Mitochondrial parameters [64] calculated from these data revealed that TAT-Cx43$_{266-283}$ decreased basal respiration and ATP-linked respiration, as well as maximal and spare respiratory capacities (Fig. 2h). Phosphorylation of ETC complexes by c-Src regulates respiration and cellular ATP content [43], which provides a mechanistic explanation for the decreased mitochondrial activity induced by TAT-Cx43$_{266-283}$—a c-Src–inhibiting peptide [17,35]—, despite no changes in the total levels of ETC complexes. Importantly, analysis of the GSC extracellular acidification rate (EACR)—mostly resulting from lactate production and hence regarded as glycolytic activity—in a

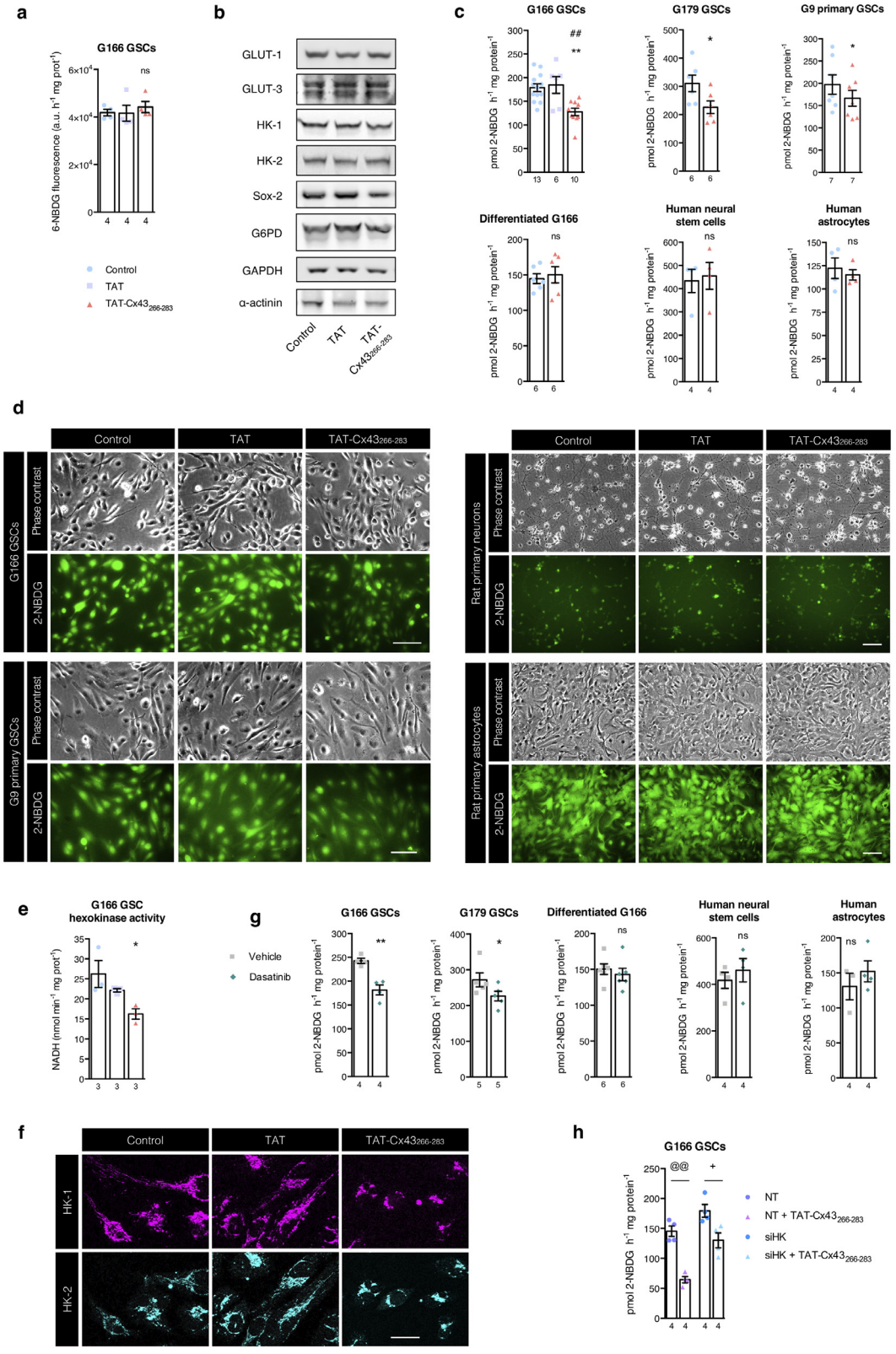

Fig. 1. TAT-Cx43$_{266-283}$ decreases glucose uptake through HK activity selectively in GSCs. Cells were treated with 50 μM TAT or TAT-Cx43$_{266-283}$ for 24 h prior to the assays where indicated. (**a**) Glucose transport was estimated with the non-phosphorylatable fluorescent glucose analogue 6-NBDG. G166 GSCs were incubated with 146 μM 6-NBDG for 1 h and lysed, and 6-NBDG fluorescence was measured in a microplate fluorometer. (**b**) Representative western blots of the indicated proteins. GAPDH and α-actinin blots are shown as loading controls. (**c**) Quantification of 2-NBDG uptake in G166 GSCs, G179 GSCs, G9 primary GSCs, differentiated G166 glioblastoma cells, human neural stem cells, and human astrocytes after TAT or TAT-Cx43$_{266-283}$ treatment. Cells were incubated with 146 μM of the fluorescent glucose analogue 2-NBDG for 1 h. (**d**) Representative micrographs showing that, while 2-NBDG uptake was not affected in neurons and astrocytes, G166 and G9 GSCs exhibited reduced 2-NBDG uptake promoted by TAT-Cx43$_{266-283}$. Scale bar: 100 μm. (**e**) Hexokinase activity in GSCs determined as described in the Methods. (**f**) G166 GSCs immunostained for HK-1 (magenta) and HK-2 (cyan). Representative micrographs showing that HK-1 and HK-2 display mostly a mitochondrial distribution and that, in GSCs treated with TAT-Cx43$_{266-283}$, HK-1 and HK-2 staining is condensed near the cell nuclei. Scale bar: 25 μm. (**g**) Quantification of 2-NBDG uptake in G166 GSCs, G179 GSCs, G9 primary GSCs, differentiated G166 glioblastoma cells, human neural stem cells and human astrocytes after

Seahorse XF analyser [64] after TAT-Cx43$_{266-283}$ treatment did not reveal any changes (Fig. 2i and Supplementary Fig. 2 g). We confirmed this result by analysing extracellular lactate in GSCs after TAT-Cx43$_{266-283}$ treatment (Fig. 2j). Recent reports show that drug resistance to standard glioblastoma therapies, such as bevacizumab, relies on the ability of cancer cells to switch their metabolism from OXPHOS to glycolysis [46]. Therefore, it is noteworthy that, despite the well-characterised ability of cancer stem cells to adapt to new metabolic requirements [4,5,50], GSCs treated with TAT-Cx43$_{266-283}$ did not show enhanced glycolysis to compensate for the decreased mitochondrial activity (Fig. 2g vs 2i). In addition, we did not find any significant effect of TAT-Cx43$_{266-283}$ on the OCR or ECAR in rat neurons or astrocytes (Supplementary Fig. 3 h), in agreement with the cell-specific effect of TAT-Cx43$_{266-283}$ [36]. Taken together, these data indicate that TAT-Cx43$_{266-283}$ downregulates mitochondrial metabolism in GSCs without increasing aerobic glycolysis, which suggests an impairment of metabolic plasticity upon TAT-Cx43$_{266-283}$ treatment.

3.3. TAT-Cx43$_{266-283}$ impairs the metabolic plasticity of GSCs

The plasticity of the metabolic phenotype of cancer stem cells is crucial in the ever-changing tumour microenvironment [4,5,46,63]. To characterise the ability of the GSCs used in this study to adapt their metabolism to shifts in nutrient availability, we used time-lapse microscopy to analyse their survival in media with different nutrient contents. Interestingly, GSCs survived for 4 days with only glucose or only amino acids in the culture medium (Fig. 3a, and Videos 1.1 and 2.1). Under these conditions, GSCs eventually adopted a dormancy state, yet they were able to resume proliferation when nutrients became available again (Fig. 3a and Videos 1.2 and 2.2), suggesting that they exhibit a high metabolic plasticity to survive to changes in nutrient availability. Notably, NSCs behaved differently when cultured in glucose-only medium: the surviving cells underwent strong changes in cell morphology and did not recover their original morphology after nutrient replenishment (Supplementary Fig. 3b), suggesting different mechanisms of response to metabolic challenges between GSCs and NSCs.

Emerging data suggest that, beyond cell-intrinsic factors, nutrient availability in the tumour microenvironment can also negatively influence drug response, hampering the efficacy of common antitumoral drugs [50]. To investigate whether this was also the case for TAT-Cx43$_{266-283}$, GSCs in complete medium were treated with 50 μM TAT or TAT-Cx43$_{266-283}$ for 24 h and then switched to glucose-only, amino acid-only, or glucose and amino acid media containing 50 μM TAT or TAT-Cx43$_{266-283}$ for a further 24 h. For comparison, GSCs were cultured in parallel in complete medium. Time-lapse microscopy and MTT assays revealed that TAT-Cx43$_{266-283}$ maintained its antitumour effect under the different nutrient-deprived conditions (Fig. 3b and c, Videos 4–9, and Supplementary Fig. 3c). Consistent with the TAT-Cx43$_{266-283}$–induced reduction in glucose uptake and metabolism, we found a pronounced increase in cell death in GSCs treated with TAT-Cx43$_{266-283}$ in glucose-only medium compared with those cultured in any other medium (Fig. 3b and c and Videos 4–9).

At the molecular level, GSCs adapted to glucose-only medium by upregulating glucose metabolism enzymes critical for cancer cells, such as HK-2 [41,63] and G6PD [65,66], a key enzyme in the pentose phosphate pathway (Supplementary Fig. 3d). However, GSCs treated with TAT-Cx43$_{266-283}$ in glucose-only medium showed markedly decreased levels of both HK-2 and G6PD, as well as GLUT-3 and, importantly, HIF-1α, a master regulator of glucose metabolism [67,68] (Fig. 3d). Meanwhile, although HK activity was decreased in GSCs treated with TAT-Cx43$_{266-283}$ in glucose-only medium (Supplementary Fig. 4e), HK-1 levels remained unchanged (Fig. 3d), suggesting that this is not a general reduction in glucose metabolism. In addition, our results confirm that TAT-Cx43$_{266-283}$ targets the metabolic adaptation to this nutrient-deprived condition because GSCs in complete medium showed no or only slight decreases in the levels of these proteins upon treatment with TAT-Cx43$_{266-283}$ for 24 h or 48 h, respectively (Fig. 1b, 3d). On a different note, Sox-2, a transcription factor implicated in stem cell maintenance [17], was also upregulated in GSCs cultured in glucose-only medium (Supplementary Fig. 3d). This is in agreement with previous studies showing cancer stem cell enrichment under nutrient-deprived conditions and the role of certain master stem cell transcription factors in promoting preferential glucose metabolism [5,69]. According to our previous results [17], Sox-2 levels in TAT-Cx43$_{266-283}$-treated GSCs were decreased in complete medium (Fig. 3d). Interestingly, here we found that this reduction also takes place in glucose-only medium, suggesting that TAT-Cx43$_{266-283}$ abrogates GSC enrichment under this condition (Fig. 3d). Together, these results indicate that GSCs treated with TAT-Cx43$_{266-283}$ fail to upregulate the proteins necessary for survival in different metabolic scenarios, particularly those needed to exploit glucose as an energy source in the absence of other nutrients (e.g., amino acids/proteins or lipids) (Fig. 3d and Supplementary Fig. 3d). This adaptation impairment might be responsible for maintaining the effect of TAT-Cx43$_{266-283}$ in different metabolic environments, in contrast to other antitumour therapies [46,50].

3.4. TAT-Cx43$_{266-283}$ impairs glucose metabolism ex vivo and in vivo

To explore the effect of TAT-Cx43$_{266-283}$ on glucose metabolism in GSCs within the brain environment, we first evaluated glucose uptake in an ex vivo model of glioblastoma [36]. As illustrated in Fig. 4a, fluorescently labelled GSCs were placed in organotypic brain slices and allowed to engraft overnight. The GSC–organotypic brain slice co-cultures were treated with 50 μM TAT or TAT-Cx43$_{266-283}$ for 48 h, incubated with 146 μM 2-NBDG in glucose-free medium for 1 h, and mounted for microscopy (Fig. 4a and b). In agreement with the in vitro 2-NBDG study (Fig. 1c and d), glucose uptake was reduced to ~65% in GSCs in co-cultures treated with TAT-Cx43$_{266-283}$ compared with control and TAT conditions (Fig. 4c and d), with no apparent effect on the brain parenchyma (Fig. 4b and d).

Next, we used an in vivo glioblastoma model consisting of the intracranial injection of 5000 fluorescently labelled human GSCs together with 100 μM TAT or TAT-Cx43$_{266-283}$ into the brains of NOD/SCID mice [36]. Seven days after surgery, the mice were sacrificed, and their brains were processed for analysis of fluorescently labelled glioma cells derived from implanted GSCs (Fig. 4e). We had already found that TAT-Cx43$_{266-283}$ impaired HK activity in vitro after 24 h of treatment (Fig. 1e) and decreased HK-2 levels and HK activity after 48 h of treatment in glucose-only medium (Fig. 3d and Supplementary Fig. 3e). We corroborated these findings in vivo through immunofluorescence analysis of HK-2 in the fluorescently labelled glioma cells of the xenografted mice, which showed a ~75% reduction in HK-2 staining in TAT-Cx43$_{266-283}$-treated mice (Fig. 4f and Supplementary Fig. 4a and b).

Within the bulk glioblastoma, GLUT-3 is preferentially expressed by GSCs in vivo and its inhibition impairs GSC growth and tumorigenicity, suggesting its value as an important target in malignant

dasatinib (1 μM; 24 h) treatment. Cells were incubated with 146 μM of the fluorescent glucose analogue 2-NBDG for 1 h. (**h**) HK-1 and HK-2 expression was silenced by siRNA in G166 GSCs (Supplementary Fig. 1f). TAT-Cx43$_{266-283}$ treatment began 48 h after silencing and 2-NBDG uptake was quantified 72 h after silencing. All data are mean ± s.e.m. ($^{*}P < 0.05$, $^{**}P < 0.01$, $^{***}P < 0.001$ vs control; $^{\#\#}P < 0.01$, $^{\#\#\#}P < 0.001$ vs TAT; @@$P < 0.01$; +$P < 0.05$; ns, not significant). Numbers under the bars indicate the number of independent experiments (**a, c, e, g, h**; each with at least two technical replicates).

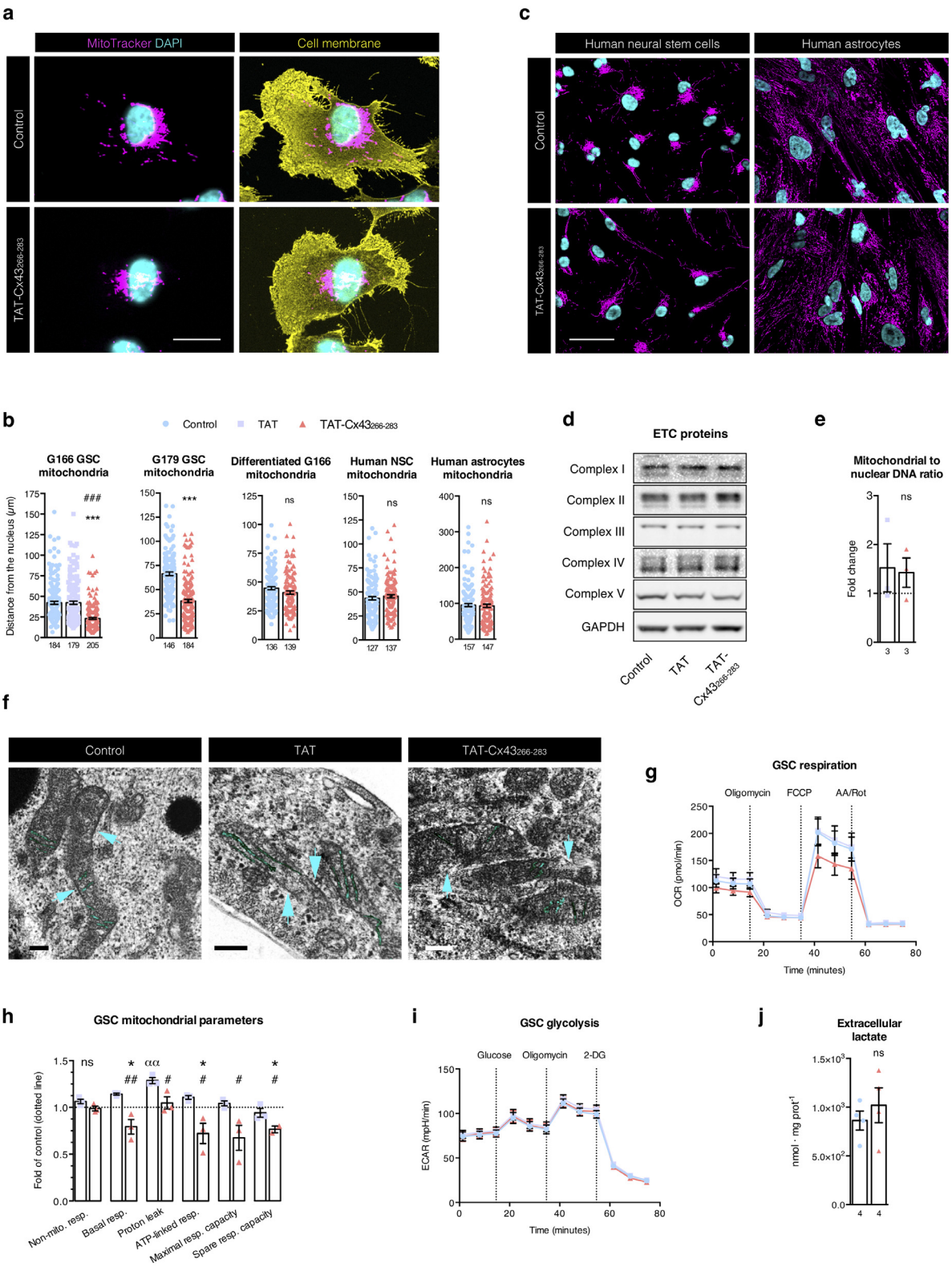

Fig. 2. TAT-Cx43$_{266-283}$ induces changes in the localisation, ultrastructure, and function of mitochondria in GSCs. GSCs were treated with 50 μM TAT or TAT-Cx43$_{266-283}$ for 24 h prior to the assays. (**a**) GSCs were incubated with MitoTracker, fixed, immunostained for GLUT-1, and imaged. Mitochondria in GSCs treated with TAT-Cx43$_{266-283}$ appeared closer to the cell nucleus and more condensed than those of control or TAT-treated GSCs. Scale bar: 20 μm. (**b**) Distance from the furthest mitochondria to the centre of the nucleus in each cell analysed. Scale bar: 50 μm. (**c**) Human neural stem cells and astrocytes were incubated with MitoTracker, fixed and imaged. TAT-Cx43$_{266-283}$ does not alter mitochondrial distribution in these cells. (**d**) Representative western blots of G166 GSCs ETC subunit proteins from complexes I (NDUFB8), II (SDHB), III (UQCRC2), IV (MTCO1), and V (ATP5A). No changes were observed in the relative levels of these mitochondrial proteins under the indicated experimental conditions. (**e**) Quantification of mitochondrial DNA relative to nuclear DNA by qPCR normalised to control (assigned a value of 1; dotted line). (**f**) GSCs were imaged with transmission electron microscopy. In GSCs treated with TAT-Cx43$_{266-283}$, the mitochondrial outer membrane and cristae were less defined, and the mitochondrial matrix was more electron-dense. Scale bar: 200 nm. (**g**) The OCR of GSCs was measured after the addition of 1.5 μM oligomycin to block ATP-linked OCR, 0.4 μM FCCP to uncouple mitochondria to the obtain the maximal OCR, and 0.5 μM rotenone/antimycin A (Rot/AA) to shut down mitochondrial respiration. Data were obtained from three independent experiments. (**h**) Quantification of mitochondrial parameters in GSCs obtained from the

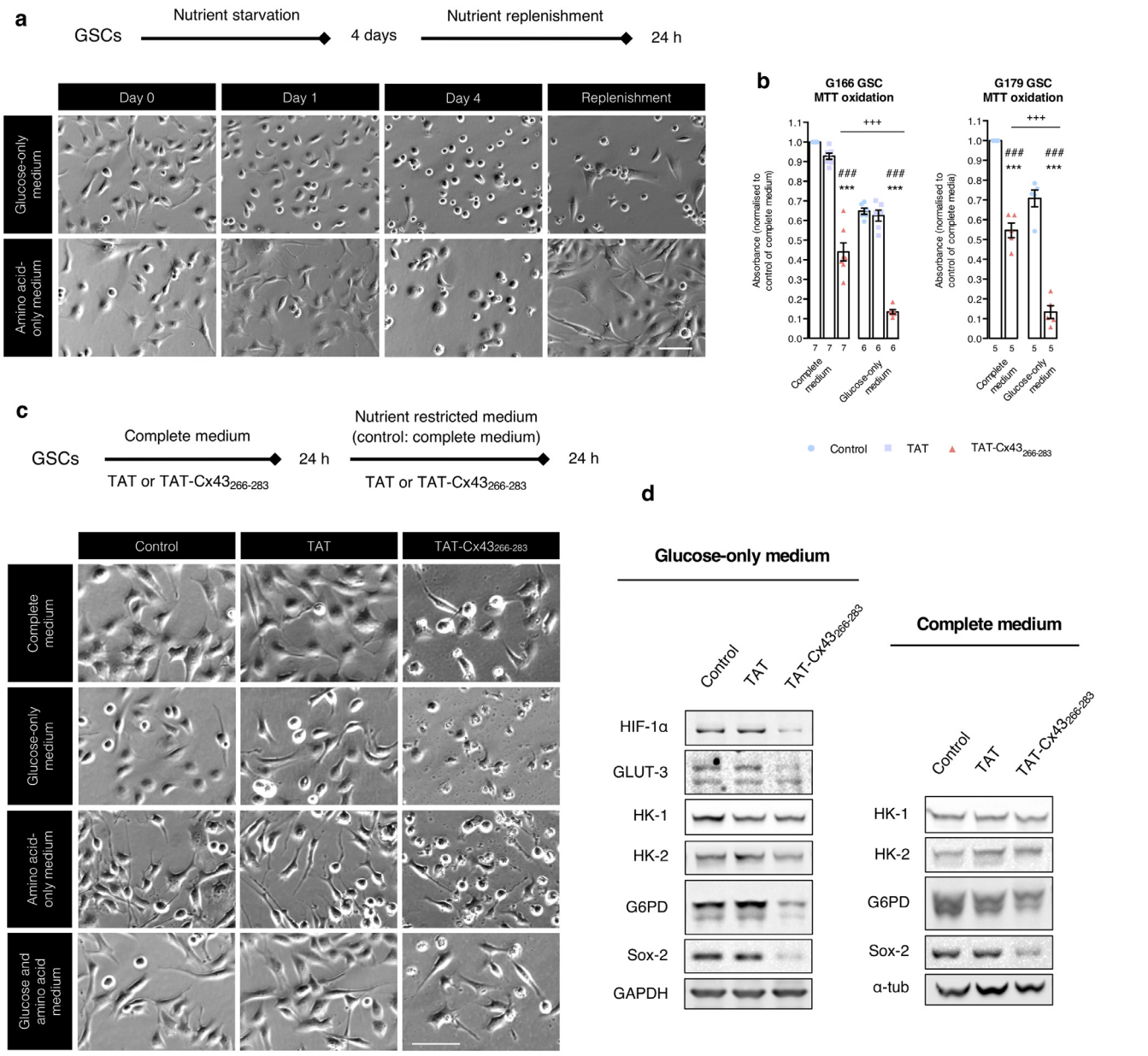

Fig. 3. TAT-Cx43$_{266-283}$ maintains its antitumour effect under several nutrient-deprived conditions. (**a**) G166 GSCs were recorded by time-lapse microscopy in medium containing only glucose or only amino acids (Videos 1 and 2, respectively). After 4 days, these media were changed to complete medium and cells were recorded for a further 24 h (nutrient replenishment). Note that cells that appeared dead (bright, round shape) could survive and proliferate after nutrient replenishment, which was not true for cells maintained in medium without any nutrients (Supplementary Fig. 3 and Video 3). Scale bar: 100 μm. (**b**–**d**) GSCs were treated with 50 μM TAT or TAT-Cx43$_{266-283}$ in complete medium for 24 h. Then, the medium was replaced with medium containing glucose (glucose-only medium), amino acids (amino acid-only medium), or both glucose and amino acids, as well as 50 μM of each peptide, for another 24 h. For comparison, cells were treated in parallel with complete medium and 50 μM of peptides. Then, the indicated assays were performed. (**b**) MTT oxidation of GSCs under the indicated conditions. (**c**) GSCs were recorded by time-lapse microscopy in complete or glucose-only medium (Videos 4–9; the images are the last photomicrograph from each video) or photographed under the indicated conditions. Scale bar: 100 μm. (**d**) Representative western blots of the indicated proteins under the indicated conditions. GSCs treated with TAT-Cx43$_{266-283}$ in glucose-only medium exhibited decreased levels of HIF-1α, GLUT-3, HK- 2, G6PD, and Sox-2, but not HK-1 (left panel). However, GSCs treated in complete medium showed only slight decreases (right panel). GAPDH and α-tubulin blots are shown as loading controls. All data are mean ± s.e.m. and were obtained from at least three independent experiments with at least two technical replicates ($^{***}P < 0.001$ vs control; $^{\#\#\#}P < 0.001$ vs TAT; $^{+++}P < 0.001$ TAT-Cx43$_{266-283}$ in glucose-only medium vs in complete medium). Numbers under the bars indicate the number of biological replicates in (**b**).

gliomas [5,62]. Because our in vitro results showed a decreased level of GLUT-3 in glucose-only medium (Fig. 3d), we analysed its level in the in vivo-implanted GSCs as well. Notably, immunofluorescence analysis revealed a ~75% reduction in GLUT-3 staining in glioma cells in TAT-Cx43$_{266-283}$-treated mice (Fig. 4g and Supplementary Fig. 4c and d). This finding and the reduced HK-2 levels in glioma cells in vivo recapitulate the HK-2 and GLUT-3 decrease found in GSCs treated in glucose-only medium in vitro (Fig. 3d).

data shown in (g) normalised to control (assigned a value of 1; dotted line). (**i**) The ECAR of GSCs was measured after the addition of 10 mM glucose to assess the glycolysis rate, 1 μM oligomycin to obtain the maximal ECAR, and 50 mM 2-deoxyglucose to shut down glycolysis. Data were obtained from four independent experiments. (**j**) Extracellular lactate measured in control and TAT-Cx43$_{266-283}$–treated GSCs. All data are mean ± s.e.m. and were obtained from at least three independent experiments (except for transmission electron microscopy images) with at least two technical replicates ($^{*}P < 0.05$ vs control, $^{***}P < 0.001$ vs control; $^{\#}P < 0.05$, $^{\#\#}P < 0.01$, $^{\#\#\#}P < 0.001$ vs TAT; $^{aa}P < 0.01$ vs TAT-Cx43; ns, not significant). Numbers under the bars indicate the number of cells analysed (**b**) or the number of biological replicates (**e** and **j**).

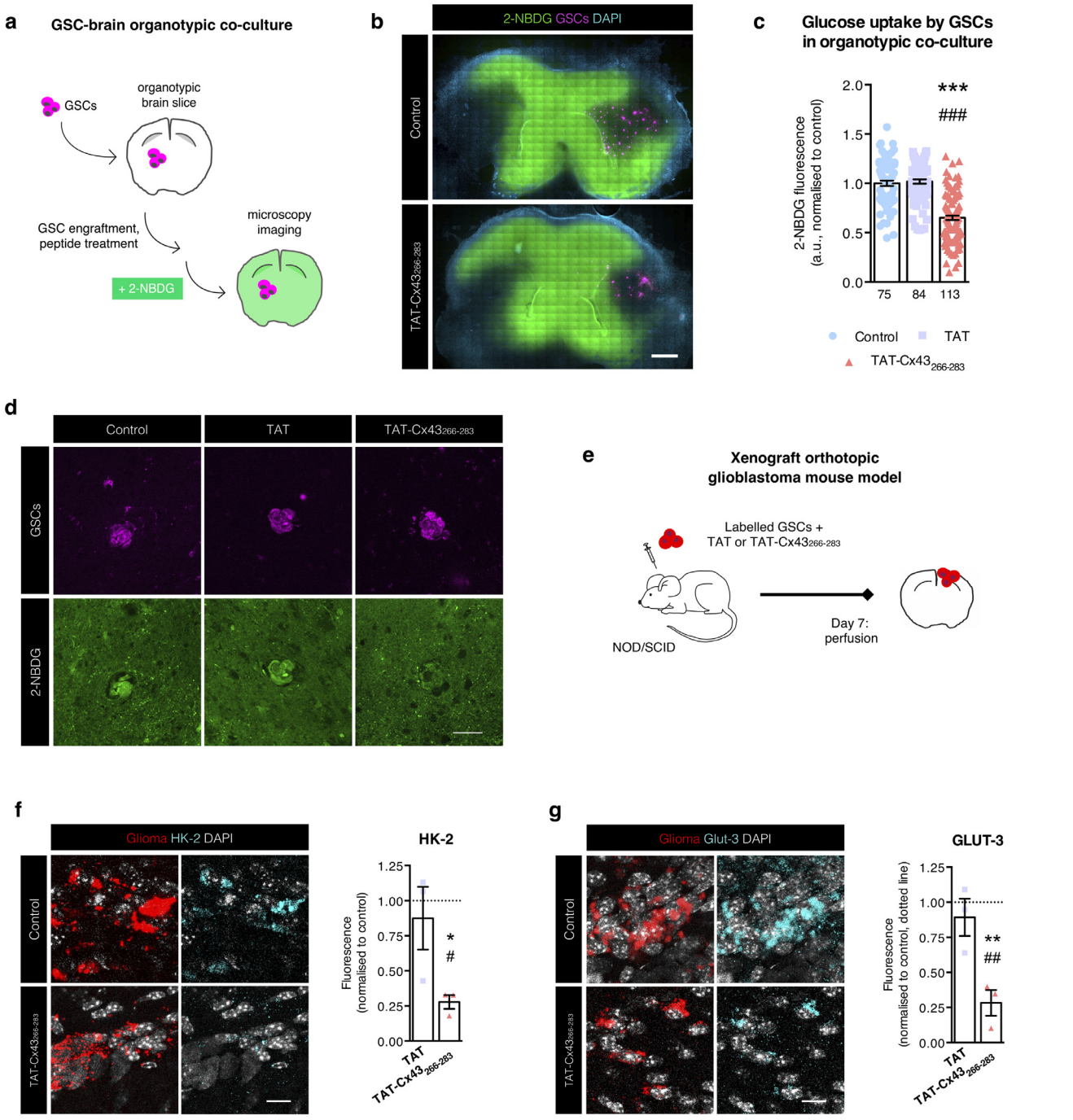

Fig. 4. TAT-Cx43$_{266-283}$ impairs glucose metabolism ex vivo and in vivo. (**a**) Schematic drawing of the 2-NBDG uptake experiments in GSC–organotypic brain slice co-cultures. A total of 2500 fluorescently labelled GSCs were placed onto each organotypic brain slice and allowed to integrate overnight. The GSC–brain slice co-cultures were incubated with 50 μM TAT or TAT-CX43$_{266-283}$ for 48 h. Then, the co-cultures were incubated with 146 μM 2-NBDG for 1 h and analysed by confocal microscopy. (**b**) Representative mosaic photomicrographs of GSC–brain slice co-cultures incubated with 146 μM 2-NBDG. Note the similar levels of 2-NBDG uptake (green) by the brain parenchyma in control and TAT-Cx43$_{266-283}$–treated co-cultures. Scale bar: 1 mm. (**c**) 2-NBDG fluorescence (mean grey value) was quantified in the ROIs corresponding to GSC fluorescence in confocal microscopy images. (**d**) Representative confocal microscopy images showing the reduction in 2-NBDG uptake (green) specifically in GSCs (magenta) in the GSC–brain slice co-cultures treated with TAT-Cx43$_{266-283}$. Scale bar: 50 μm. (**e**) Schematic drawing of the in vivo experimental design. Briefly, 5000 human GSCs fluorescently labelled with PKH26 or constitutively expressing mCherry were intracranially injected alone (control) or together with 100 μM TAT or TAT-Cx43$_{266-283}$ into the brains of NOD/SCID mice. After 7 days, the animals were perfused, and their brains were processed for immunofluorescence and analysed by confocal microscopy. (**f** and **g**) Representative images of control and TAT-Cx43$_{266-283}$ brain sections of a xenograft mouse model of glioma showing implanted glioma cells (**f** and **g;** shown in red) and HK-2 (**f**; shown in cyan) or GLUT-3 (**g**; shown in cyan). Scale bar: 50 μm. See Supplementary Fig. 4. for the specificity of antibodies against human HK-2 and GLUT-3. Quantification of HK-2 and GLUT-3 fluorescence is shown next to each panel. Mean fluorescence intensity was normalised to control (assigned a value of 1; dotted line). Three animals were analysed per condition. Data are mean ± s.e.m. and were obtained from at least three independent experiments ($^{*}P < 0.05$, $^{**}P < 0.01$, $^{***}P < 0.001$ vs control; $^{\#}P < 0.05$, $^{\#\#}P < 0.01$, $^{\#\#\#}P < 0.001$ vs TAT). Numbers under the bars indicate the number of ROIs analysed in (**c**).

4. Discussion

Our previous studies showed that GSCs can be specifically targeted by a short cell-penetrating peptide based on Cx43 (TAT-$Cx43_{266-283}$) that reduces tumour growth in preclinical models [36] via c-Src inhibition [17]. In primary GSCs and freshly removed surgical specimens studied as undissociated glioblastoma blocks, TAT-$Cx43_{266-283}$ dramatically reduced growth, migration, and survival [35]. The effects of TAT-$Cx43_{266-283}$ on GSC metabolism found in this study highlight the therapeutic potential of this compound against glioblastoma because TAT-$Cx43_{266-283}$ targets crucial proteins for glioblastoma malignancy, namely GLUT-3, HK-2, G6PD, and HIF-1α [5,41,62,63,65-67,70]. Our in vitro, ex vivo, and in vivo data show that glucose uptake is specifically impaired in GSCs through short- and long-term mechanisms involving the regulation of the activity and expression of key glucose enzymes. Indeed, our results suggest an initial short-term regulation of HK activity, presumably through inhibition of its phosphorylation by c-Src [41]. This is followed by long-term regulation through reduced HK-2 protein levels, which is highly relevant considering the strong link between HK activity, particularly that of HK-2, and the malignant phenotype [41,63]. We hypothesise that, because c-Src activity stabilises the levels of HIF-1α [39,40], TAT-$Cx43_{266-283}$ might decrease HIF-1α through c-Src inhibition, leading to the downstream downregulation of HK-2, G6PD, and GLUT-3 shown here. In agreement with these results, Cx43 has been proposed to regulate glucose uptake and the expression of HK-2 and GLUT-3 through c-Src and HIF-1α [39]. In addition, TAT-$Cx43_{266-283}$ increases the levels of PTEN in G166, G9, and other primary GSCs [35], which could also contribute to blocking HIF-1α–dependant gene transcription [71].

GLUT-3 has been identified as an excellent target to reduce glioblastoma progression because of the high dependence of GSCs on this glucose transporter [5,62]. However, in the brain context, the inhibition of GLUT-3 is challenging because it is also the main glucose transporter in neurons [72]. Remarkably, we found that TAT-$Cx43_{266-283}$ downregulates GLUT-3 in GSCs without affecting glucose uptake in neurons, probably because its regulation in neurons is independent of c-Src activity [72]. In fact, TAT-$Cx43_{266-283}$ appears to be innocuous in terms of neural stem cell, neuronal and astrocytic metabolism, presumably because of the low basal activity of c-Src in healthy cells [17].

A growing body of work indicates that GSCs oxidise glucose and other substrates via OXPHOS as a primary energy source, for which they require an intact mitochondrial respiratory chain to survive and sustain stemness and tumorigenic potential [73-76]. As previously mentioned, c-Src, via phosphorylation of ETC complexes, regulates the mitochondrial respiration necessary for the survival of glioblastoma cells [43]. Consistent with these reports, here we show that the c-Src inhibiting peptide TAT-$Cx43_{266-283}$ impairs glucose mitochondrial metabolism and promotes GSC death. Moreover, ATP generated in the ETC is necessary for the c-Src–activating phosphorylation at Y416 [77,78], which might create a negative regulatory loop if ATP becomes scarce due to TAT-$Cx43_{266-283}$-induced decreased glucose uptake. In terms of glioblastoma therapy, the impairment of mitochondrial metabolism is remarkable because it might per se increase the effectiveness of radiotherapy [8]. Importantly, the reduced mitochondrial activity promoted by TAT-$Cx43_{266-283}$ is not compensated by an increase in glycolysis, which is critical to avoid drug resistance [46,48,50]. Indeed, TAT-$Cx43_{266-283}$ exerts antitumour effects in different nutrient-depleted media, where it prevents metabolic plasticity and eventually leads to cell death. This is especially relevant considering the growing body of work acknowledging intrinsic and extrinsic metabolic states as key factors in cancer drug resistance [46,47,50,79].

Although further research is needed to address the role of TAT-$Cx43_{266-283}$ in amino acid, lipid, and protein metabolism, our in vivo work shows that the effects of TAT-$Cx43_{266-283}$ on GSC metabolism extend beyond the in vitro conditions, indicating that they are independent of the metabolic tumour microenvironment, in contrast to other antitumoral drugs [50]. The metabolically challenging tumour environment promotes GSC enrichment [5-7]. However, TAT-$Cx43_{266-283}$ reduces GLUT-3 and HK-2 levels in GSCs in vivo, proteins which are heavily involved in cancer establishment, maintenance, and resistance [5,41,62,63,70]. Concomitantly, in the same glioblastoma model used in this study, TAT-$Cx43_{266-283}$ induces the loss of the stemness phenotype of the implanted GSCs, as shown by decreased expression of Sox-2 and nestin in these cells 7 days post-implantation, and impairs glioblastoma growth 30 days post-implantation, leading to decreased tumorigenicity and increased survival [36]. Given our in vitro, ex vivo, and in vivo results and the fundamental role played by HK-2 [41,63] and GLUT-3 [5] in glioblastoma formation and development, TAT-$Cx43_{266-283}$, by inhibiting c-Src, might impair in vivo glioblastoma growth through both the loss of the stemness phenotype [36] and the abrogation of metabolic plasticity, two phenomena that are highly dynamic and tightly linked [4-7,9].

Previous studies from our group showed increased glucose uptake in rat astrocytes by the inhibition of Cx43-gap junctional communication [80] through a mechanism involving microtubules, suggesting that changes in the cytoskeleton could participate in the effects of TAT-$Cx43_{266-283}$ on glucose uptake. However, TAT-$Cx43_{266-283}$ affects actin but not tubulin distribution in GSCs [81]. Furthermore, while the inhibition of Src with dasatinib exerted a similar effect to TAT-$Cx43_{266-283}$ on glucose uptake, the disruption of actin polymerisation with latrunculin A did not modify the rate of glucose uptake (data not shown). These results suggest that changes in the cytoskeleton are probably not involved in glucose uptake in human GSCs. Hence, although other mechanisms might contribute, we propose that the inhibition of c-Src promoted by TAT-$Cx43_{266-283}$ could be the link between all the effects on GSC metabolism found in this study.

In the context of immunotherapy, one hallmark of T-cell activation, which is necessary for the immune response, is a profound metabolic remodelling that highly resembles that of cancer cells [82]. However, according to early work, T-cell expression of HK-2 [83] or GLUT-3 [84] is dispensable for T-cell activation. Moreover, HK-2 expression in lung cancer cells is correlated positively with expression of programmed death-ligand 1 (PD-L1), an immune checkpoint that allows tumour cells to evade immune surveillance, and negatively with interferon gamma secretion by T-cells [85]. These results suggest that targeting HK-2 or GLUT-3 in combination with immunotherapy might reverse tumour immunosuppression and produce beneficial outcomes in cancer therapy.

From a clinical point of view, the search for therapeutic molecules that specifically target the metabolism of cancer stem cells is on the rise [86], with metabolic plasticity and the nutrient composition of the tumour microenvironment at the centre of the drug response [50]. Taken together, our results support the notion that metabolic plasticity, rather than specific metabolic pathways, constitutes a major targetable vulnerability [4], and confirm the value of TAT-$Cx43_{266-283}$ for glioblastoma therapy alone or in combination with other therapies, including those whose resistance relies on metabolic adaptation.

Funding sources

This work was supported by the Spanish Ministerio de Economía y Competitividad (FEDER BFU2015-70040-R and FEDER RTI2018-099873-B-I00) and Fundación Ramón Areces. S. G. Pelaz, M. Jaraíz-Rodríguez, A. Álvarez-Vázquez and R. Flores-Hernández are fellowship recipients from the Junta de Castilla y León and the European Social Fund. L. García-Vicente is a fellowship recipient from the

Spanish Ministerio de Ciencia and R. Talaverón is a postdoctoral fellowship recipient from the Asociación Española Contra el Cáncer (AECC). The corresponding author had full access to all the data in the study and had final responsibility for the decision to submit for publication.

Author contributions

S.G.P. contributed to the experimental design and development, data acquisition, and analysis and interpretation of all of the experiments, and drafted the article. S.G.P., M.J.-R., R.T., and L.G.-V. performed the in vivo experiments. A.Á-V. helped in western blotting experiments and hexokinase activity and 2-NBDG uptake assays. L. G.-V. performed the TAT-Cx43$_{266-283}$-B internalization experiment. R.F.-H. helped in cell culture. M.G.C., M.T., and A.R.M. helped to design, acquire, and process the data from the Seahorse experiments and supervised them. C.L. processed the samples for electron microscopy analysis and obtained and interpreted the images. J.M.M. contributed to the experimental design and data interpretation. A.T. conceived and designed the experiments, supervised the experimental development and analysis, interpreted the data, and drafted the article. All of the co-authors revised the article for important intellectual content and approved the final version for publication.

Declaration of Competing Interest

The authors declare no competing interests.

Acknowledgements

We thank T. del Rey (University of Salamanca) for the technical assistance, C. Ljurko, M. Romo-González, and Á. Hernández (University of Salamanca) for helping with the qPCR experiments, and the Microscopy Service of the *Centro de Investigación del Cáncer* (CIC-IBMCC, Salamanca) for helping with confocal image acquisition.

Supplementary materials

Supplementary material associated with this article can be found, in the online version, at doi:10.1016/j.ebiom.2020.103134.

References

[1] Gilbert MR, et al. A randomized trial of bevacizumab for newly diagnosed glioblastoma. N Engl J Med 2014;370:699–708. doi: 10.1056/NEJMoa1308573.
[2] Chen J, et al. A restricted cell population propagates glioblastoma growth after chemotherapy. Nature 2012;488:522–6. doi: 10.1038/nature11287.
[3] Bao S, et al. Glioma stem cells promote radioresistance by preferential activation of the DNA damage response. Nature 2006;444:756–60. doi: 10.1038/nature05236.
[4] Dirkse A, et al. Stem cell-associated heterogeneity in Glioblastoma results from intrinsic tumor plasticity shaped by the microenvironment. Nat Commun 2019;10:1787. doi: 10.1038/s41467-019-09853-z.
[5] Flavahan WA, et al. Brain tumor initiating cells adapt to restricted nutrition through preferential glucose uptake. Nat Neurosci 2013;16:1373–82. doi: 10.1038/nn.3510.
[6] Hjelmeland AB, et al. Acidic stress promotes a glioma stem cell phenotype. Cell Death Differ 2011;18:829–40. doi: 10.1038/cdd.2010.150.
[7] Heddleston JM, Li Z, McLendon RE, Hjelmeland AB, Rich JN. The hypoxic microenvironment maintains glioblastoma stem cells and promotes reprogramming towards a cancer stem cell phenotype. Cell Cycle 2009;8:3274–84. doi: 10.4161/cc.8.20.9701.
[8] Vlashi E, et al. Metabolic state of glioma stem cells and nontumorigenic cells. Proc Natl Acad Sci U S A 2011;108:16062–7. doi: 10.1073/pnas.1106704108.
[9] Peiris-Pages M, Martinez-Outschoorn UE, Pestell RG, Sotgia F, Lisanti MP. Cancer stem cell metabolism. Breast Cancer Res 2016;18:55. doi: 10.1186/s13058-016-0712-6.
[10] Snyder V, Reed-Newman TC, Arnold L, Thomas SM, Anant S. Cancer stem cell metabolism and potential therapeutic targets. Front Oncol 2018;8:203. doi: 10.3389/fonc.2018.00203.
[11] Sancho P, Barneda D, Heeschen C. Hallmarks of cancer stem cell metabolism. Br J Cancer 2016;114:1305–12. doi: 10.1038/bjc.2016.152.
[12] Dando I, et al. The metabolic landscape of cancer stem cells. IUBMB Life 2015;67:687–93. doi: 10.1002/iub.1426.
[13] Huang RP, Hossain MZ, Sehgal A, Boynton AL. Reduced connexin43 expression in high-grade human brain glioma cells. J Surg Oncol 1999;70:21–4. doi: 10.1002/(sici)1096-9098(199901)70:1<21::aid−jso4>3.0.co;2-0.
[14] Pu P, Xia Z, Yu S, Huang Q. Altered expression of Cx43 in astrocytic tumors. Clin Neurol Neurosurg 2004;107:49–54. doi: 10.1016/j.clineuro.2004.03.006.
[15] Yu SC, et al. Connexin 43 reverses malignant phenotypes of glioma stem cells by modulating E-cadherin. Stem Cells 2012;30:108–20. doi: 10.1002/stem.1685.
[16] Hitomi M, et al. Differential connexin function enhances self-renewal in glioblastoma. Cell Rep 2015;11:1031–42. doi: 10.1016/j.celrep.2015.04.021.
[17] Gangoso E, Thirant C, Chneiweiss H, Medina JM, Tabernero A. A cell-penetrating peptide based on the interaction between c-Src and connexin43 reverses glioma stem cell phenotype. Cell Death Dis 2014;5:e1023. doi: 10.1038/cddis.2013.560.
[18] Zhu D, Caveney S, Kidder GM, Naus CCG. Transfection of C6 glioma-cells with connexin-43 cDNA - analysis of expression, intercellular coupling, and cell-proliferation. Proc Natl Acad Sci USA 1991;88:1883–7.
[19] Naus CCG, Elisevich K, Zhu DG, Belliveau DJ, Delmaestro RF. In vivo growth of C6 glioma-cells transfected with Connexin43 cDNA. Cancer Res 1992;52:4208–13.
[20] Aasen T, et al. Connexins in cancer: bridging the gap to the clinic. Oncogene 2019;38:4429–51. doi: 10.1038/s41388-019-0741-6.
[21] Oliveira R, et al. Contribution of gap junctional communication between tumor cells and astroglia to the invasion of the brain parenchyma by human glioblastomas. BMC Cell Biol 2005;6:7. doi: 10.1186/1471-2121-6-7.
[22] Lin JH, et al. Connexin 43 enhances the adhesivity and mediates the invasion of malignant glioma cells. J Neurosci 2002;22:4302–11 20026450.
[23] Gielen PR, et al. Connexin43 confers Temozolomide resistance in human glioma cells by modulating the mitochondrial apoptosis pathway. Neuropharmacology 2013;75:539–48. doi: 10.1016/j.neuropharm.2013.05.002.
[24] Grek CL, et al. Novel approach to temozolomide resistance in malignant glioma: connexin43-directed therapeutics. Curr Opin Pharmacol 2018;41:79–88.
[25] Murphy SF, et al. Connexin 43 inhibition sensitizes chemoresistant glioblastoma cells to temozolomide. Cancer Res 2016;76:139–49.
[26] Leithe E, Mesnil M, Aasen T. The connexin 43 C-terminus: a tail of many tales. Biochim Biophys Acta 2018;1860:48–64. doi: 10.1016/j.bbamem.2017.05.008.
[27] Gonzalez-Sanchez A, et al. Connexin43 recruits PTEN and Csk to inhibit c-Src activity in glioma cells and astrocytes. Oncotarget 2016;7:49819–33. doi: 10.18632/oncotarget.10454.
[28] Herrero-Gonzalez S, et al. Connexin43 inhibits the oncogenic activity of c-Src in C6 glioma cells. Oncogene 2010;29:5712–23. doi: 10.1038/onc.2010.299.
[29] Tabernero A, Gangoso E, Jaraíz-Rodríguez M, Medina JM. The role of connexin43-Src interaction in astrocytomas: a molecular puzzle. Neuroscience 2016;323:183–94. doi: 10.1016/j.neuroscience.2015.02.029.
[30] Du J, et al. Bead-based profiling of tyrosine kinase phosphorylation identifies SRC as a potential target for glioblastoma therapy. Nat Biotechnol 2009;27:77–83. doi: 10.1038/nbt.1513.
[31] Han X, et al. The role of Src family kinases in growth and migration of glioma stem cells. Int J Oncol 2014;45:302–10. doi: 10.3892/ijo.2014.2432.
[32] Liu C, et al. The interaction between cancer stem cell marker CD133 and Src protein promotes focal adhesion kinase (FAK) phosphorylation and cell migration. J Biol Chem 2016;291:15540–50. doi: 10.1074/jbc.M115.712976.
[33] Singh S, et al. EGFR/Src/Akt signaling modulates Sox2 expression and self-renewal of stem-like side-population cells in non-small cell lung cancer. Mol Cancer 2012;11:73. doi: 10.1186/1476-4598-11-73.
[34] Wei, Y. et al. Activation of PI3K/Akt pathway by CD133-p85 interaction promotes tumorigenic capacity of glioma stem cells. 110, 6829−34, doi:10.1073/pnas.1217002110 (2013).
[35] Jaraiz-Rodriguez M, et al. A short region of Connexin43 reduces human glioma stem cell migration, invasion, and survival through Src, PTEN, and FAK. Stem Cell Rep 2017;9:451–63. doi: 10.1016/j.stemcr.2017.06.007.
[36] Jaraíz-Rodríguez M, et al. Connexin43 peptide, TAT-Cx43266-283, selectively targets glioma cells, impairs malignant growth and enhances survival in mouse models in vivo. Neuro Oncol 2019. doi: 10.1093/neuonc/noz243.
[37] Flier JS, Mueckler MM, Usher P, Lodish HF. Elevated levels of glucose transport and transporter messenger RNA are induced by ras or src oncogenes. Science 1987;235:1492–5.
[38] Jain S, et al. Src inhibition blocks c-Myc translation and glucose metabolism to prevent the development of breast cancer. Cancer Res 2015;75:4863–75. doi: 10.1158/0008-5472.CAN-14-2345.
[39] Valle-Casuso JC, Gonzalez-Sanchez A, Medina JM, Tabernero A. HIF-1 and c-Src mediate increased glucose uptake induced by Endothelin-1 and Connexin43 in Astrocytes. PLoS ONE 2012;7:e32448. PONE-d-11-18920 [pii]. doi: 10.1371/journal.pone.0032448.
[40] Karni R, Dor Y, Keshet E, Meyuhas O, Levitzki A. Activated pp60c-Src leads to elevated hypoxia-inducible factor (HIF)-1alpha expression under normoxia. J Biol Chem 2002;277:42919–25. doi: 10.1074/jbc.M206141200.
[41] Zhang J, et al. c-Src phosphorylation and activation of hexokinase promotes tumorigenesis and metastasis. Nat Commun 2017;8:13732. doi: 10.1038/ncomms13732.
[42] Pan S, World CJ, Kovacs CJ, Berk BC. Glucose 6-phosphate dehydrogenase is regulated through c-Src-mediated tyrosine phosphorylation in endothelial cells. Arterioscler Thromb Vasc Biol 2009;29:895–901. doi: 10.1161/ATVBAHA.109.184812.
[43] Ogura M, Yamaki J, Homma MK, Homma Y. Mitochondrial c-Src regulates cell survival through phosphorylation of respiratory chain components. Biochem J 2012;447:281–9. doi: 10.1042/BJ20120509.

[44] Miyazaki T, Neff L, Tanaka S, Horne WC, Baron R. Regulation of cytochrome c oxidase activity by c-Src in osteoclasts. J Cell Biol 2003;160:709–18. doi: 10.1083/jcb.200209098.
[45] Yoshida S, et al. Molecular chaperone TRAP1 regulates a metabolic switch between mitochondrial respiration and aerobic glycolysis. Proc Natl Acad Sci U S A 2013;110:E1604–12. doi: 10.1073/pnas.1220659110.
[46] Fack F, et al. Bevacizumab treatment induces metabolic adaptation toward anaerobic metabolism in glioblastomas. Acta Neuropathol 2015;129:115–31. doi: 10.1007/s00401-014-1352-5.
[47] Miranda-Gonçalves V, et al. Metabolic alterations underlying Bevacizumab therapy in glioblastoma cells. Oncotarget 2017;8:103657–70. doi: 10.18632/oncotarget.21761.
[48] Palm W, et al. The utilization of extracellular proteins as nutrients is suppressed by mTORC1. Cell 2015;162:259–70. doi: 10.1016/j.cell.2015.06.017.
[49] Muir A, et al. Environmental cystine drives glutamine anaplerosis and sensitizes cancer cells to glutaminase inhibition. Elife 2017;6. doi: 10.7554/eLife.27713.
[50] Muir A, Vander Heiden MG. The nutrient environment affects therapy. Science 2018;360:962–3. doi: 10.1126/science.aar5986.
[51] Okawa S, et al. Proteome and secretome characterization of glioblastoma-derived neural stem cells. Stem Cells 2017;35:967–80. doi: 10.1002/stem.2542.
[52] Pollard SM, et al. Glioma stem cell lines expanded in adherent culture have tumor-specific phenotypes and are suitable for chemical and genetic screens. Cell Stem Cell 2009;4:568–80. doi: 10.1016/j.stem.2009.03.014.
[53] Hook L, et al. Non-immortalized human neural stem (NS) cells as a scalable platform for cellular assays. Neurochem Int 2011;59:432–44. doi: 10.1016/j.neuint.2011.06.024.
[54] Tabernero A, Orfao A, Medina JM. Astrocyte differentiation in primary culture followed by flow cytometry. Neurosci Res 1996;24:131–8. doi: 10.1016/0168-0102(95)00981-7.
[55] Gump JM, Dowdy SF. TAT transduction: the molecular mechanism and therapeutic prospects. Trends Mol Med 2007;13:443–8. doi: 10.1016/j.molmed.2007.08.002.
[56] Polo-Hernández E, et al. Oleic acid synthesized by stearoyl-CoA desaturase (SCD-1) in the lateral periventricular zone of the developing rat brain mediates neuronal growth, migration and the arrangement of prospective synapses. Brain Res 2014;1570:13–25. doi: 10.1016/j.brainres.2014.04.038.
[57] Barros LF, et al. Kinetic validation of 6-NBDG as a probe for the glucose transporter GLUT1 in astrocytes. J Neurochem 2009;109(Suppl 1):94–100. doi: 10.1111/j.1471-4159.2009.05885.x.
[58] Schindelin J, et al. Fiji: an open-source platform for biological-image analysis. Nat Methods 2012;9:676–82. doi: 10.1038/nmeth.2019.
[59] Kleaveland B, Shi CY, Stefano J, Bartel DP. A network of noncoding regulatory RNAs acts in the mammalian brain. Cell 2018;174:350–62 e317. doi: 10.1016/j.cell.2018.05.022.
[60] Rooney JP, et al. PCR based determination of mitochondrial DNA copy number in multiple species. Methods Mol Biol 2015;1241:23–38. doi: 10.1007/978-1-4939-1875-1_3.
[61] Pfaffl MW. A new mathematical model for relative quantification in real-time RT-PCR. Nucleic Acids Res 2001;29:e45. doi: 10.1093/nar/29.9.e45.
[62] Cosset É, et al. Glut3 addiction is a druggable vulnerability for a molecularly defined subpopulation of glioblastoma. Cancer Cell 2017;32:856–68 e855. doi: 10.1016/j.ccell.2017.10.016.
[63] Wolf A, et al. Hexokinase 2 is a key mediator of aerobic glycolysis and promotes tumor growth in human glioblastoma multiforme. J Exp Med 2011;208:313–26. doi: 10.1084/jem.20101470.
[64] Pike Winer LS, Wu M. Rapid analysis of glycolytic and oxidative substrate flux of cancer cells in a microplate. PLoS ONE 2014;9:e109916. doi: 10.1371/journal.pone.0109916.
[65] Kuo W, Lin J, Tang TK. Human glucose-6-phosphate dehydrogenase (G6PD) gene transforms NIH 3T3 cells and induces tumors in nude mice. Int J Cancer 2000;85:857–64. doi: 10.1002/(sici)1097-0215(20000315)85:6<857::aid−ijc20>3.0.co;2-u.
[66] Ju HQ, et al. Disrupting G6PD-mediated Redox homeostasis enhances chemosensitivity in colorectal cancer. Oncogene 2017;36:6282–92. doi: 10.1038/onc.2017.227.
[67] Singh D, et al. Overexpression of hypoxia-inducible factor and metabolic pathways: possible targets of cancer. Cell Biosci 2017;7:62. doi: 10.1186/s13578-017-0190-2.
[68] Denko NC. Hypoxia, HIF1 and glucose metabolism in the solid tumour. Nat Rev Cancer 2008;8:705–13. doi: 10.1038/nrc2468.
[69] Vardhana SA, et al. Glutamine independence is a selectable feature of pluripotent stem cells. Nat Metab 2019;1:676–87. doi: 10.1038/s42255-019-0082-3.
[70] Patra KC, et al. Hexokinase 2 is required for tumor initiation and maintenance and its systemic deletion is therapeutic in mouse models of cancer. Cancer Cell 2013;24:213–28. doi: 10.1016/j.ccr.2013.06.014.
[71] Zhong H, et al. Modulation of hypoxia-inducible factor 1alpha expression by the epidermal growth factor/phosphatidylinositol 3-kinase/PTEN/AKT/FRAP pathway in human prostate cancer cells: implications for tumor angiogenesis and therapeutics. Cancer Res 2000;60:1541–5.
[72] Ferreira JM, Burnett AL, Rameau GA. Activity-dependent regulation of surface glucose transporter-3. J Neurosci 2011;31:1991–9. doi: 10.1523/JNEUROSCI.1850-09.2011.
[73] Janiszewska M, et al. Imp2 controls oxidative phosphorylation and is crucial for preserving glioblastoma cancer stem cells. Genes Dev 2012;26:1926–44. doi: 10.1101/gad.188292.112.
[74] Lin H, et al. Fatty acid oxidation is required for the respiration and proliferation of malignant glioma cells. Neuro Oncol 2017;19:43–54. doi: 10.1093/neuonc/now128.
[75] Marin-Valencia I, et al. Analysis of tumor metabolism reveals mitochondrial glucose oxidation in genetically diverse human glioblastomas in the mouse brain in vivo. Cell Metab 2012;15:827–37. doi: 10.1016/j.cmet.2012.05.001.
[76] Park HK, et al. Interplay between TRAP1 and Sirtuin-3 modulates mitochondrial respiration and oxidative stress to maintain stemness of glioma stem cells. Cancer Res 2019;79:1369–82. doi: 10.1158/0008-5472.CAN-18-2558.
[77] Park JH, et al. Fatty acid oxidation-driven Src links mitochondrial energy reprogramming and oncogenic properties in triple-negative breast cancer. Cell Rep 2016;14:2154–65. doi: 10.1016/j.celrep.2016.02.004.
[78] Arachiche A, et al. Localization of PTP-1B, SHP-2, and Src exclusively in rat brain mitochondria and functional consequences. J Biol Chem 2008;283:24406–11. doi: 10.1074/jbc.M709217200.
[79] Intlekofer AM, Finley LWS. Metabolic signatures of cancer cells and stem cells. Nat Metab 2019;1:177–88. doi: 10.1038/s42255-019-0032-0.
[80] Sánchez-Alvarez R, Tabernero A, Medina JM. Endothelin-1 stimulates the translocation and upregulation of both glucose transporter and hexokinase in astrocytes: relationship with gap junctional communication. J Neurochem 2004;89:703–14. doi: 10.1046/j.1471-4159.2004.02398.x.
[81] Jaraiz-Rodriguez M, Gonzalez-Sanchez A, Garcia-Vicente L, Medina JM, Tabernero A. Biotinylated cell-penetrating peptides to study intracellular protein-protein interactions. J Vis Exp 2017. doi: 10.3791/56457.
[82] Le Bourgeois T, et al. Targeting T cell metabolism for improvement of cancer immunotherapy. Front Oncol 2018;8:237. doi: 10.3389/fonc.2018.00237.
[83] Mehta MM, et al. Hexokinase 2 is dispensable for T cell-dependent immunity. Cancer Metab 2018;6:10. doi: 10.1186/s40170-018-0184-5.
[84] Macintyre AN, et al. The glucose transporter Glut1 is selectively essential for CD4 T cell activation and effector function. Cell Metab 2014;20:61–72. doi: 10.1016/j.cmet.2014.05.004.
[85] Kim S, et al. Programmed cell death ligand-1-mediated enhancement of hexokinase 2 expression is inversely related to T-cell effector gene expression in non-small-cell lung cancer. J Exp Clin Cancer Res 2019;38:462. doi: 10.1186/s13046-019-1407-5.
[86] Wong TL, Che N, Ma S. Reprogramming of central carbon metabolism in cancer stem cells. Biochim Biophys Acta Mol Basis Dis 2017;1863:1728–38. doi: 10.1016/j.bbadis.2017.05.012.